Experimental implementation of a Pyramid WFS: Towards the first SCAO systems for E-ELT

C. Z. Bond[a], K. El Hadi[a], J. F. Sauvage[a,b], C. Correia[a], O.Fauvarque[a], D. Rabaud[c], B. Neichel[a], and T. Fusco[a,b]

[a]Aix Marseille Université, CNRS, Laboratoire d'Astrophysique de Marseille, UMR 7326, 13388, Marseille, France
[b]ONERA, Optics department, 29 avenue de la Division Leclerc, 92322 Châtillon, France
[c]Innovation Network, 13580, La Fare les Olliviers, France

ABSTRACT

Investigations into the Pyramid wavefront sensor (P-WFS) have experimentally demonstrated the ability to achieve a better performance than with a standard Shack-Hartmann sensor (SH-WFS). Implementation on the Large Binocular Telescope (LBT) provided the first operational demonstration on a facility-class instrument of a P-WFS on sky. The desire to implement a Pyramid on an Extremely Large Telescope (ELT) requires further characterisation in order to optimise the performance and match our knowledge and understanding of other wave-front sensors (WFSs).

Within the framework of the European Extremely Large Telescope (E-ELT), the Laboratoire d'Astrophysique de Marseille (LAM) is involved in the preparation of the Single Conjugate Adaptive Optics (SCAO) system of HARMONI, E-ELT's 1st light integral field spectrograph (IFU). The current baseline WFS for this adaptive optics system is a Pyramid WFS using a high speed and sensitive OCAM2 camera. At LAM we are currently carrying out laboratory demonstrations of a Pyramid-WFS, with the aim to fully characterise the behaviour of the Pyramid in terms of sensitivity and linear range. This will lead to a full operational procedure for the use of the Pyramid on-sky, assisting with current designs and future implementations. The final goal is to provide an on sky comparison between the Pyramid and Shack-Hartmann at Observatoire de la Côte d'Azur (OCA). Here we present our experimental setup and preliminary results.

Keywords: E-ELT, Adaptive Optics, Pyramid WFS, OCAM2 camera

1. INTRODUCTION

The Laboratoire d'Astrophysique de Marseille (LAM) is involved in the development of adaptive optics systems for future large telescopes, in particular towards the European Extremely Large Telescope (E-ELT). Within this framework we are carrying out a full investigation into a Pyramid wave-front sensor (P-WFS), a cutting edge sensor in terms of high order, high sensitivity wave-front sensing.[1] Previous investigations have demonstrated the potential for a better performance than the classic Shack-Hartmann WFS, in terms of sensitivity and aliasing rejection.[2] In addition compelling results from the implementation of a P-WFS on the Large Binocular Telescope[3] has lead to the inclusion of the Pyramid in the baseline of many future large telescopes, including the single conjugate adaptive optics (SCAO) system of the HARMONI instrument on E-ELT.[4]

To successfully implement a P-WFS on future extremely large telescopes requires further knowledge of the Pyramid behaviour. At LAM we aim to complete a full investigation of the P-WFS: from understanding the principles and behaviour in theory, and using numerical simulations, to a full experimental characterisation of the sensor. The final goal is an on-sky comparison with the Shack-Hartmann at Observatoire de la Côte d'Azur (OCA). Here we present our latest results: initial tests of the P-WFS signals in preparation for full closed loop measurements.

Corresponding author: C. Z. Bond
E-mail: charlotte.bond@lam.fr

2. EXPERIMENTAL SETUP

A Pyramid wave-front sensor consists a glass prism, the Pyramid, onto which a pupil plane light field is focused. The 4 facets of the prism project 4 distinct images of the pupil onto a CCD camera, via a re-imaging lens. The design of the LAM Pyramid sensor using an OCAM2 CCD camera has previously been presented.[5–8]

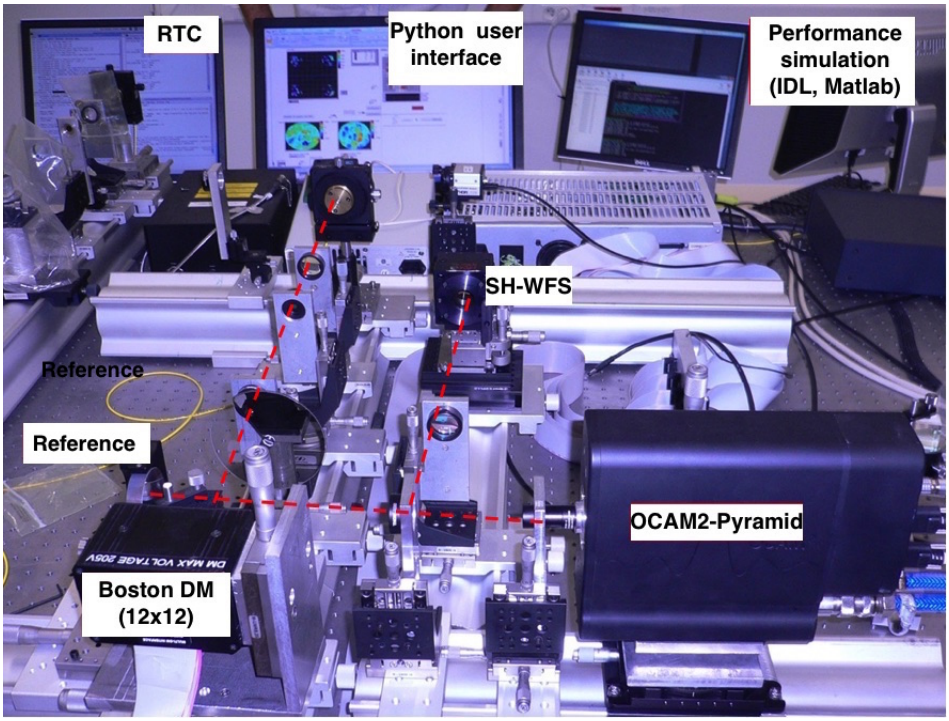

Figure 1. Photograph showing the optical setup of the LAM Pyramid bench. A pupil is applied to a LASER light source which then is incident on a deformable mirror and reference mirror, by means of a beam-splitter. Either mirror can be blocked off. The light is then sent to two wave-front sensors, the Pyramid sensor and HASO Shack-Hartmann sensor. The light for the Pyramid sensor is focused onto the tip of prism, whilst the HASO sits at a conjugate pupil plane.

The optical setup of the Pyramid experimental bench at LAM is illustrated in figure 1. The setup consists of a laser, pupil, flat reference mirror, a 12×12 deformable mirror (DM), the Pyramid sensor and an HASO Shack-Hartmann sensor (32×32 lenlets). Additionally beam-splitters and lenses are used to direct and shape the beam, ensuring the pupil and focal planes fall at the correct positions (i.e. pupil plane at DM and focal plane on the tip of the Pyramid). The optical setup allows operation either with the DM or a flat reference mirror, which is used for calibration and reference signals. The Shack-Hartmann (SH-WFS) is used to flatten the DM before our initial Pyramid measurements and aides in alignment and centring of the pupil on the DM. Subsequently we will take parallel measurements with the SH-WFS and P-WFS, comparing the performance of the Pyramid with this classical sensor.

The Pyramid and DM are controlled by an RTC (real time controller) provided by Shaktiware which processes the Pyramid signals, computing the wave-front signals from the pupil images. The RTC controls the shape of DM by applying voltages to the individual actuators, which is then used to compute the interaction matrix between the DM actuators and Pyramid signals. The RTC will then be used to control the adaptive optics loop during real time operation.

The pupil images generated by the Pyramid WFS are processed by the RTC to produce the Pyramid signals. Only the valid region of the pupils is used to calculate these signals and the centring and alignment of the pupils is crucial to produce the correct signals. The valid pupil areas and the equivalent pixel in each pupil is illustrated in figure 2. Unlike the Shack-Hartmann the signals of the P-WFS are not pure slope measurements

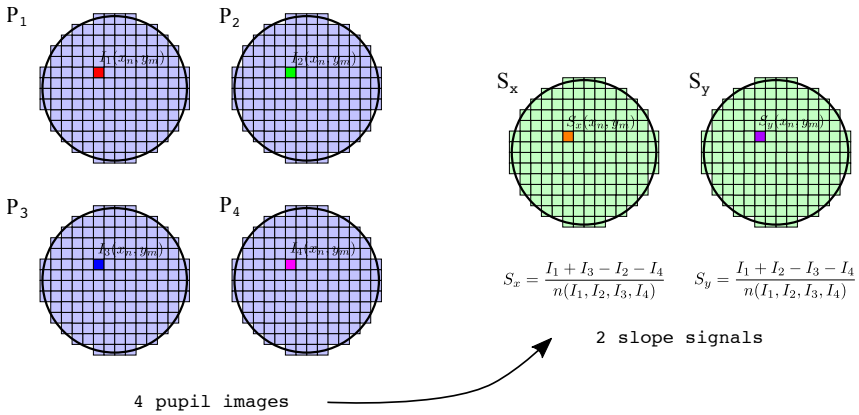

Figure 2. Diagrams illustrating the valid and equivalent pixels in the 4 pupil images and slope signals. $I_k(x_n, y_m)$ refers to the intensity in the kth pupil and equivalent $[n, m]$ pixel. S_x and S_y refer to the slope signals and n is a normalisation function dependent on the 4 pupil images.

and, depending on the modulation, can act as a direct phase measurement for high order distortions.[2] The computation of the Pyramid signals is a linear combination of the pupil images which are normalised to avoid any dependence on the laser intensity. For the signal in x we have:

$$S_x(x, y) = \frac{I_1 + I_3 - I_2 - I_4}{n(I_1, I_2, I_3, I_4)} \tag{1}$$

and for y:

$$S_y(x, y) = \frac{I_1 + I_2 - I_3 - I_4}{n(I_1, I_2, I_3, I_4)} \tag{2}$$

where I_n refer to the intensity maps of the 4 pupils, as shown in figure 2 and n is a normalisation factor, a function of the 4 pupil images. The formation of n is not trivial and can have a large impact on the theoretical and practical implementation of the signal. The choice of normalisation forms one of our initial tests of the system, as is detailed in section 3.1.

3. EXPERIMENTAL AND SIMULATION RESULTS

In preparation for the full closed loop study several initial measurements were taken to check the response of the Pyramid and calibrate the interaction between the deformable mirror and Pyramid wave-front sensor. Explicitly this involves tests of the linearity of the Pyramid signals, in which we revisit the choice of normalisation, and measurements of the interaction matrix. These test also involve a comparison with a numerical model of the Pyramid, developed in parallel in IDL (Interactive Data Language).

3.1 Choice of normalisation

The classical normalisation of the Pyramid signals, as expressed in,[1] uses a pixel-wise normalisation: every signal pixel is normalised by the total intensity in that pixel, summed across the four pupils:

$$S_x = \frac{I_1 + I_3 - I_2 - I_4}{I_1 + I_2 + I_3 + I_4} \qquad S_y = \frac{I_1 + I_2 - I_3 - I_4}{I_1 + I_2 + I_3 + I_4} \tag{3}$$

However, depending on the phase regime, the denominator can vary strongly across the pupil, with some pixels registering relatively high intensities whilst others give signals close to zero. This variation will create noisy variations in the slope, adding unwanted signals to the measurement. We therefore defined a second normalisation using a 'flat map' normalisation, where the flat map is the average intensity over the 4 pupils and valid pixels:

$$S_x = \frac{I_1 + I_3 - I_2 - I_4}{\frac{1}{A}\int_A [I_1 + I_2 + I_3 + I_4] \mathrm{d}A} \qquad S_y = \frac{I_1 + I_2 - I_3 - I_4}{\frac{1}{A}\int_A [I_1 + I_2 + I_3 + I_4] \mathrm{d}A} \tag{4}$$

where A is the valid area covered by the pupil images. Effectively this normalisation is a constant. This provides a normalisation which avoids dependence on the phase regime, especially in the case of strong phase values where pyramid linearity is known to present a limited range. Moreover, this normalisation is equal to the average flux values, avoiding the opportunity for close to 0 values and preventing the addition of unwanted, noisy information into the signals.

At LAM we have configured the RTC on the Pyramid bench to work for both normalisations, with the ability to easily switch between the two methods. In the next section we will analyse the signals generated using each method, for a poke of the central DM actuator.

3.2 Linearity tests

Before fully calibrating the interaction between the DM and the P-WFS we first check the linearity of the signals to the poke of an individual DM actuator. This is a necessary step before we take the interaction matrix as we must ensure the matrix is taken within the linear range of the sensor. Within these tests we compare the response of the two normalisation methods.

In preparation for our linearity tests we first flatten the DM using the HASO signal. The Pyramid signals from this flattened DM will form a reference measurement which is removed from all subsequent wave-front measurements, providing the 0 point:

$$S_{\text{Pym.}} = S_\phi - S_0 \tag{5}$$

where $S_{\text{Pym.}}$ is the final Pyramid signal, S_ϕ is the raw signal for any phase distortion and S_0 is a reference signal measured with a flattened DM.

To test the linearity we apply a ramp of voltage to one of the central DM actuators, applying this on top of the 'flattening voltage'. In order to assess the validity of our results simulations of the setup were carried out in IDL. The presence of a calibrated HASO on the optical bench allows for realistic comparisons between simulation and experiment, as the HASO measurement of the DM surface (and poke) is used as an input in our model, feeding it with this measured poke shape.

Some of the signals from this measurement are summarised in figure 3 for both normalisation methods and for a range of actuator poke. The two different methods produce quite different signal shapes. For pixel-wise normalisation the signal is more widely spread. We also note that in some cases the shape of the signal (for pixel-wise normalisation) looks quite different from experiment to simulation. The flat normalisation, on the other hand, produces narrow, distinct signals which appear in both the measurement and simulation. This is due to the pixel-wise method whose normalisation increases the impact of small intensity signals where the average intensity across the pupils (and hence normalisation) is relatively small. Since these small effects are likely to be the greatest differences between the experiment and simulation we observe significant differences between the two results. Such an effect is avoided with the flat map.

Already we can see that the pixel-wise normalisation appears to plateau quickly, with the signal maps shown in figure 3 having similar amplitudes away from the zero point. To get plots of the linearity we chose a simple metric: we record the maximum and minimum of the Pyramid signals and see how these vary with actuator stroke. The results are shown in figure 4 for both S_x and S_y and for the pixel-wise normalisation (top) and flat-map normalisation (bottom). In each case the experimental and simulated results are shown. These plots illustrate differences in the linear range depending on the normalisation we use: the linear range using the flat-map method is significantly larger.

3.3 Preparation for closing the loop: Measuring the interaction matrix

In preparation for operating the P-WFS in a full closed loop we first measure the interaction matrix between the DM actuators and Pyramid signals. This measurement is controlled by the RTC which acts on each actuator, producing a positive and negative stroke to fully calibrate the response of the system. For each actuator the corresponding signals are recorded and stored in the interaction matrix. Again we collect the results for the two normalisation methods.

Figure 5 shows plots of the interaction matrices. An interaction matrix is a $N_{\text{act}} \times N_{\text{slopes}}$ martix, where N_{act} is the number of actuators and N_{slopes} is the number of wave-front sensor slope measurements. In this case

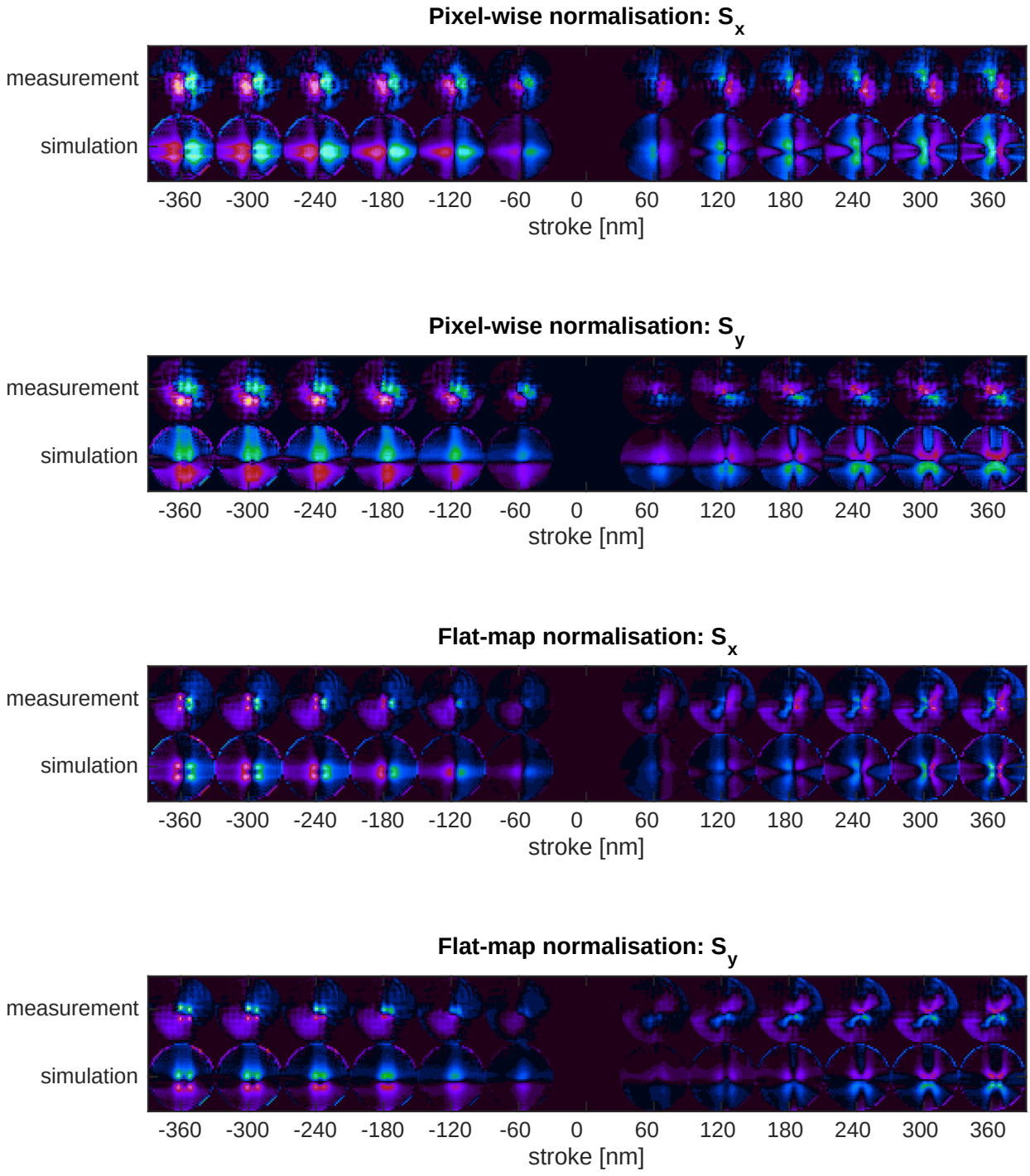

Figure 3. Plots showing the Pyramid signals for an individual actuator poke, for a range of poke amplitudes. From top to bottom: x and y signals for pixel-wise normalisation and x and y signals for flat-map normalisation.

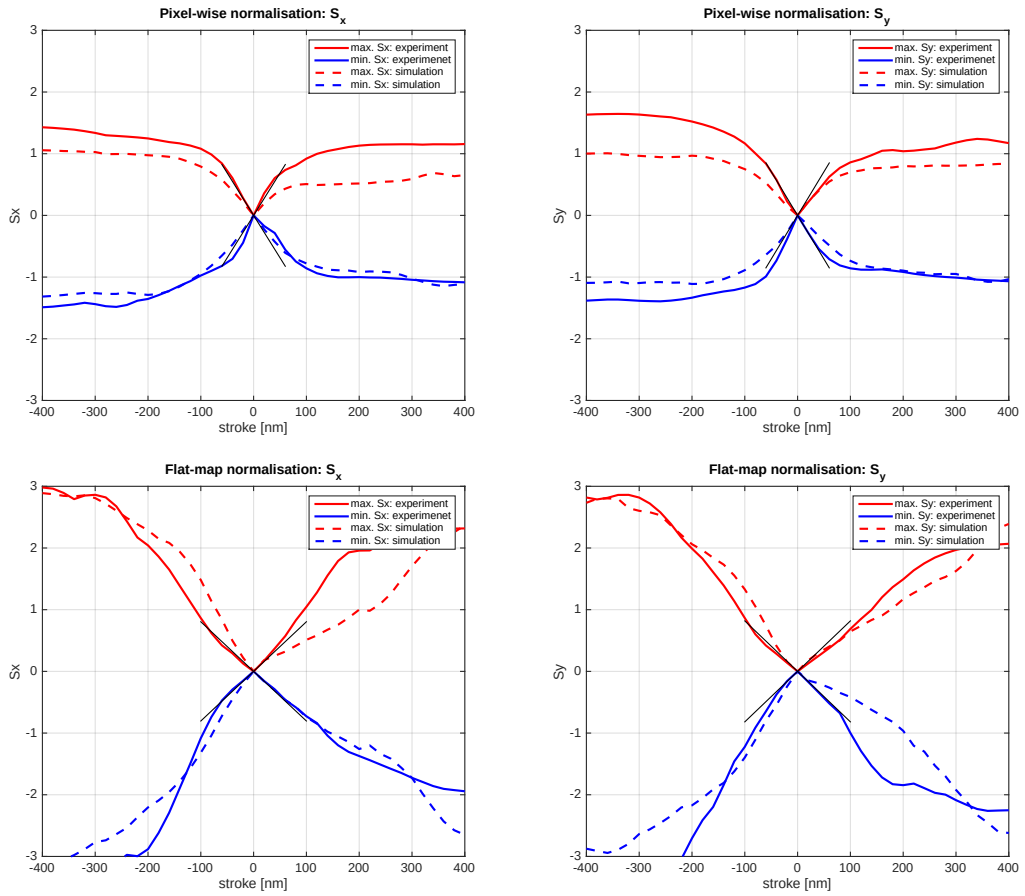

Figure 4. Plots showing the Pyramid signals for an individual actuator poke, for a range of poke amplitudes. The x (left) and y (right) signals are shown for two different normalisations, a pixel-wise normalisation (top) and a flat-map normalisation (bottom). In each case the results from the experiment and from simulations are shown. The black cross plotted across the centre of each figure shows the average linear relationship in each plot.

N_{slopes} is the twice the number of valid pixels within the pyramid pupil images on the CCD, incoperating the 2 matrices for the x and y signals. The values of the matrix are the slope signal (S_x and S_y) at the given pixel (k) when an individual actuator (j) is poked, normalised by poke amplitude a_p:

$$I[j,k] = \frac{1}{a_p} \begin{bmatrix} S_x[k] \\ S_y[k] \end{bmatrix} \tag{6}$$

During the measurement the amplitude of the actuator poke is chosen to be within the linear range of the system, as investigated in section 3.2.

Figure 5 shows the interaction matrices measured for the two normalisations, for an actuator poke of $a_p = 0.08\lambda$. In the case of the pixel-wise normalisation the interaction is more spread out than the flat normalisation, as previously observed with an individual actuator poke. The pixel-wise case normalises by the average intensity in each pixel, resulting in a strongly varying normalisation which can reduce the signal at points of high intensity and increase the signal for low intensity measurements. The result of this is that the signal is spread over more sensor pixels. The flat map method normalises by a constant and so the interaction maintains a stronger signal where the distortion (in this case the DM actuator) is strong and little signal away from the distortion.

To better compare the two matrices we perform a singular-value-decomposition (SVD). The SVD is a process of inverting the interaction matrix which allows us to extract the eigenmodes (deformable mirror modes) of the

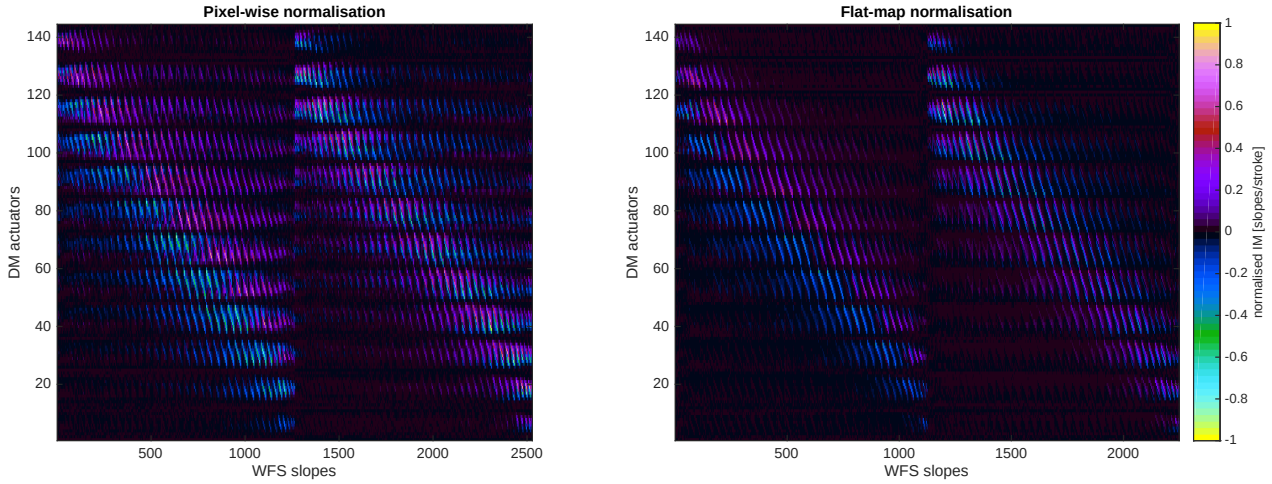

Figure 5. Plots of the interaction matrices between DM actuators and P-WFS signals for pixel-wise normalisation (left) and flat-map normalisation (right). In each plot the x signals are shown on the left, the y on right.

system and the equivalent eigenvalues (the sensitivity of the system to a given eigenmode). This analysis allows us to more easily compare our two methods in terms of sensitivity. The SVDs are shown in figure 6. Here the normalised eigenvalues are plotted for the given eigenmode. Overall these plots illustrate that the flat map normalisation provides greater sensitivity over the controllable modes. In practice this inversion is truncated to a given number of modes, avoiding those the system is least sensitive to. Modes seen very weakly by the system can produce erroneously large signals when inverted, truncating such modes avoids this at the expense of no control of these particular DM modes. A chosen figure of merit is often the conditioning number, the ratio between the eigenvalues for the first and last modes in the truncated series. A conditioning number of 1 would give equal sensitivity to all possible eiegmodes. In the SVDs shown in figure 6 the conditioning number for both methods is around 1000, when all modes are included, with the flat map method proving slightly worse. However, we will truncate in practice and due to the higher sensitivity exhibited over most modes the flat-map normalisation will allow us to:

- Increase the number of controlled modes for a given conditioning number.
- Achieve a better conditioning number for a given number of controlled modes.

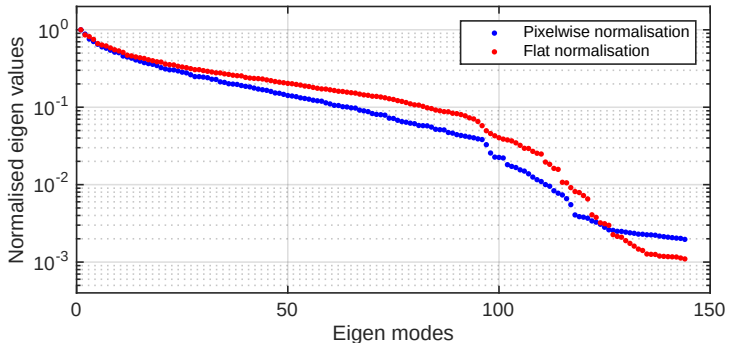

Figure 6. Singular value decomposition corresponding to the interaction matrices shown in figure 5. The results are shown for a pixel-wise normalisation and flat normalisation.

4. CONCLUSION AND OUTLOOK

Initial tests and calibrations of the Pyramid bench at LAM, incorporating an OCAM2 camera, have been completed. We have tested the static response of the Pyramid, specifically to the action of an individual DM actuator, revisiting the choice of signal normalisation. In addition we also compared the experimental measurements with simulation results. These tests demonstrate a flat normalisation, using the average total intensity, provides a greater linear range and more distinct signals than the classical pixel-wise normalisation. Furthermore, in preparation for performing closed loop tests interaction matrices between DM actuators and P-WFS signals were measured. Through a singular-value-decomposition analysis these results also illustrated a superior performance using a flat normalisation, showing greater sensitivity across most of the correctable modes. With these interaction matrices measured we are now prepared to close the loop in the laboratory with the non-modulated Pyramid.

The next step in this investigation is to extend our investigation to include modulation, using a fast tip-tilt mirror to introduce the modulation, synchronised with the OCAM2 camera. For the modulated closed loop system we will implement a gain tracking loop to optimise performance. Finally, using the ONERA-ODISSEE bench at Observatoire de la Cte d'Azur (OCA), we plan to perform on-sky tests in mid 2016. The aim is to carry out a complete comparison between the Shack-Hartmann and the Pyramid performance, with both sensors based on the same OCAM2 detector.

ACKNOWLEDGMENTS

The work presented in this paper has been done in collaboration with J. L. Gach (LAM,FLI) and F. Chazalet (SHAKTI) and was supported by the French CSA-ASHRA, ONERA-NAIADE and European FP7 OPTICON programs. This research is supported by the A*MIDEX project (no. ANR-11-IDEX-0001-02) funded by the French Government program 'Investissements d'Avenir" and managed by the French National Research Agency (ANR).

REFERENCES

[1] Ragazzoni, R., "Pupil plane wavefront sensing with an oscillating prism," *Journal of Modern Optics* **43**(2), 289–293 (1996).

[2] Vérinaud, C., "On the nature of the measurements provided by a pyramid wave-front sensor," *Optics Communications* **233**(1-3), 27–38 (2004).

[3] Esposito, S., Riccardi, A., Fini, L., Pinna, E., Puglisi, A., Quiros, F., Xompero, M., Briguglio, R., Busoni, L., Stefanini, P., Arcidiacono, C., Brusa, G., and D.Miller, "LBT AO on-sky results," in [*AO4ELT-II*], (2011).

[4] Niranjan, A. et al., "HARMONI: the first light integral field spectrograph for the E-ELT," in [*SPIE 9147*], (2014).

[5] El Hadi, K., Fusco, T., and Le Roux, B., "Toward an experimental validation of new AO concepts for future E-ELT instrumentation," in [*SPIE 8447*], (2012).

[6] El Hadi, K., Gray, M., Fusco, T., and Le Roux, B., "New wavefront sensing concepts for adaptive optics instrumentation," in [*SPIE 8535*], (2012).

[7] El Hadi, K., Fusco, T., Sauvage, J. F., and Neichel, B., "High speed and high precision pyramid wavefront sensor. in labs validation and preparation to on sky demonstration," in [*SPIE 9148*], (2014).

[8] El Hadi, K., Vignaux, M., and Fusco, T., "Development of a pyramid wavefront sensor," in [*AO4ELT-III*], (2015).